Human Molecular Genetics, 2008, Vol. 17, No. 13 ***1877–1889***
doi:10.1093/hmg/ddn083
Advance Access published on March 12, 2008

Different cellular and molecular mechanisms for early and late-onset myelin protein zero mutations

Marina Grandis[1,*], Tiziana Vigo[1,3], Mario Passalacqua[2], Manisha Jain[4], Sara Scazzola[3], Veronica La Padula[1], Michelle Brucal[4], Federica Benvenuto[1], Lucilla Nobbio[1], Angela Cadoni[2], Gian Luigi Mancardi[1], John Kamholz[4], Michael E. Shy[4] and Angelo Schenone[1,3]

[1]Department of Neurosciences, Ophthalmology and Genetics and [2]Department of Experimental Medicine, University of Genova, 16132 Genova, Italy, [3]Institute of Molecular Bioimaging and Physiology, (IBFM)-Section of Genova, Italian National Research Council, 16132 Genova, Italy and [4]Department of Neurology and Center for Molecular Medicine and Genetics, Wayne State University, Detroit, MI 48201, USA

Received February 19, 2008; Revised February 19, 2008; Accepted March 10, 2008

Mutations in the gene MPZ, encoding myelin protein zero (MPZ), cause inherited neuropathies collectively called Charcot–Marie–Tooth type 1B (CMT1B). Based on the age of onset, clinical and pathological features, most MPZ mutations are separable into two groups: one causing a severe, early-onset, demyelinating neuropathy and a second, causing a late-onset neuropathy with prominent axonal loss. To investigate potential pathomechanisms underlying the two phenotypes, we transiently transfected HeLa cells with two late-onset (T95M, H10P) and two early-onset (H52R, S22_W28 deletion) mutations and analyzed their effects on intracellular protein trafficking, glycosylation, cell viability and intercellular adhesion. We found that the two late-onset mutations were both transported to the cell membrane and moderately reduced MPZ-mediated intercellular adhesion. The two early-onset mutations caused two distinct abnormalities. H52R was correctly glycosylated and trafficked to the plasma membrane, but strongly affected intercellular adhesion. When co-expressed with wild-type MPZ (wtMPZ), a functional dominant negative effect was observed. Alternatively, S22_W28 deletion was retained within the cytoplasm and reduced both adhesion caused by wtMPZ and cellular viability. Since the same trafficking patterns were observed in transfected murine Schwann cells, they are not an artifact of heterologous cell expression. Our results suggest that at least some late-onset mutations cause a partial loss of function in the transfected cells, whereas multiple abnormal gain of function pathways can result in early-onset neuropathy. Further characterization of these pathways will lead to a better understanding of the pathogenesis of CMT1B and a rational basis for treating these debilitating inherited neuropathies.

INTRODUCTION

Myelin protein zero (MPZ), the major structural protein of peripheral nervous system (PNS) myelin, is a homotypic adhesion molecule necessary for normal myelin compaction (1–4). MPZ is the simplest member of the immunoglobulin supergene family, and consists of three structural domains: a single 124 amino acid immunoglobulin-like extracellular domain; a 26 amino acid transmembrane domain; and a 69 amino acid intracellular domain. Exon 1 encodes a 29 amino signaling protein that targets MPZ to the myelin sheath (1). Because these 29 amino acids are cleaved prior to insertion of the protein into the myelin sheath, they are not present in the mature MPZ protein and are not included in the subsequent numbering system of amino acids in this manuscript. Post-translational modifications occur as the protein is trafficked from the endoplasmic reticulum (ER) to the Schwann cell plasma membrane by addition of a single N-linked oligosaccharide at N93, as well by the addition of sulfate, acyl and phosphate groups (4).

Crystallographic analysis of the MPZ extracellular domain suggests that the protein interacts within the plane of the

*To whom correspondence should be addressed. Tel: +39 0103537057; Fax: +39 0103538639; Email: mgrandis@neurologia.unige.it

© *The Author 2008. Published by Oxford University Press. All rights reserved.*
For Permissions, please email: journals.permissions@oxfordjournals.org

membrane to form a lattice of homotetramers, each of which then interacts with similar structures on the opposing myelin loops to mediate myelin compaction (5). The cytoplasmic domain of MPZ is also necessary for its adhesive function, since deletion of the C-terminal 28 amino acids, including a putative PKCα target site, abolishes MPZ-mediated adhesion *in vitro* (6–7). Recent data shows that this portion of the protein interacts directly with both RACK1 and PKCα to regulate phosphorylation and homotypic adhesion, demonstrating that MPZ, like other Ig superfamily members, participates in a signal transduction cascade (8).

Mutations in *MPZ* gene cause the autosomal dominant peripheral neuropathy, Charcot–Marie–Tooth disease type 1B (CMT1B). More than 120 different mutations have been identified in all three domains of the mature protein, although the majority of mutations are within the extracellular, Ig-like domain. Interestingly, most patients with neuropathy caused by *MPZ* mutations can be separated into two distinct groups: one in which disease onset occurs in infancy, the clinical disability is relatively severe, and nerve conduction velocities (NCVs) are slow; and a second in which disease onset occurs in adulthood, usually after age 40, the clinical disability is relatively mild, and NCVs are essentially normal (9). Morphological studies of these early- and late-onset forms of CMT1B have demonstrated distinct molecular and pathological abnormalities (10–11), although the molecular mechanisms underlying these differences have not been identified.

To investigate the molecular pathogenesis of CMT1B, we expressed four different MPZ mutants in HeLa cells by transient transfection and then analyzed intracellular trafficking, glycosylation, cell surface expression, cell viability and MPZ-mediated homotypic adhesion of transfected proteins. The mutations we selected for this analysis included two late-onset mutants, H10P and T95M, and two early-onset mutants, S22_W28 deletion (S22_W28del) and H52R (9). We found that the two mutations causing late-onset neuropathy were both transported normally to the HeLa cell plasma membrane and slightly reduced MPZ-mediated intercellular adhesion. One of the two mutations that caused early-onset neuropathy, however, S22_W28del, was retained in the ER and did not reach the cell surface, while the other, H52R, was transported normally. Both these mutant proteins significantly decreased MPZ-mediated adhesion. Since these same trafficking patterns were observed after transfection of primary cultures of murine Schwann cells, they are not an artifact of heterologous cell expression. Taken together these data suggest that the molecular mechanisms causing early- and late-onset CMT1B are different. In the cases of late-onset CMT1B, the mutant proteins reach the cell surface but only minimally reduce MPZ adhesion, suggesting that they are incorporated into the myelin sheath where they alter axonal–glial interactions. In contrast, in the early-onset CMT1B caused by S22_W28del, the mutant protein does not reach the cell surface but significantly reduces MPZ-mediated adhesion, suggesting that it is not incorporated into myelin and so produces its effects by a gain of function mechanism. Since in the early-onset CMT1B caused by H52R, the protein both reaches the cell surface and significantly effects adhesion, it is probably incorporated into myelin but produces its effect through a dominant-negative mechanism. The two CMT1B phenotypes are thus produced by at least three distinct genetic mechanisms, demonstrating the complexity of the pathogenesis of this disease.

RESULTS

Mutations causing late-onset CMT1B do not disrupt intracellular trafficking

In order to investigate the intracellular trafficking of mutant proteins causing a late-onset disease, we transiently transfected HeLa cells with both a wild-type MPZ-DsRed fusion and either of two MPZ mutant-EGFP constructs which cause late-onset neuropathy, T95M and H10P. The intracellular localization of these proteins was then evaluated by confocal microscopy performed 24 h after the transfections. Both the wild-type MPZ-DsRed (wtMPZ-DsRed) and the wild-type MPZ- Enhanced Green Fluorescent Protein (wtMPZ-EGFP) fusion proteins reached the plasma membrane in singly and co-transfected cells, demonstrating that neither the DsRed nor EGFP tags interacted to prevent normal trafficking of MPZ (data not shown). Proteins encoding the T95M and H10P mutations fused to EGFP also co-localized with wtMPZ-DsRed (R_R *0.85*; H10P: R_R 0.88), suggesting that both mutant proteins reached the plasma membrane and did not interfere with trafficking of the wild-type protein (Fig. 1). Using a surface biotinylation assay to quantitate MPZ expression on the plasma membrane of transfected cells, we also showed that the relative surface expression of each of the two mutant proteins was essentially the same as that of the wild-type MPZ (wtMPZ: 0.75; T95M: 0.75; and H10P: 0.68), confirming our qualitative results. These data thus demonstrate that two mutant forms of MPZ, T95M and H10P, which cause late-onset neuropathy, are both transported to the plasma membrane at comparable levels with that of wild-type MPZ, and do not prevent normal intracellular transport of the wild-type protein through the ER and the Golgi to the plasma membrane.

The two MPZ mutants causing early-onset neuropathy have different patterns of intracellular expression

In order to investigate the intracellular trafficking of mutant MPZ causing early-onset disease, we also transiently transfected HeLa cells with both a wtMPZ-DsRed and either of two MPZ mutant-EGFP constructs which cause early-onset neuropathy, S22_W28del and H52R. Confocal imaging demonstrated that the H52R-EGFP fusion protein was correctly transported to the plasma membrane (R_R 0.87) along with the wild-type protein (Fig. 1), and these results were confirmed by surface biotinylation assay in which the relative surface expression of both wtMPZ-EGFP and H52R mutant were essentially identical (0.70 versus 0.75).

In contrast, the mutant S22_W28del-EGFP fusion was not transported to the cell surface (R_R 0.50), but was retained within the HeLa cell cytoplasm, probably within the ER. Expression of S22_W28del-EGFP, however, did not interfere with the normal intracellular transport of the wtMPZ-DsRed fusion (Fig. 1). These results were confirmed by biotinylation assay, since the relative surface expression of

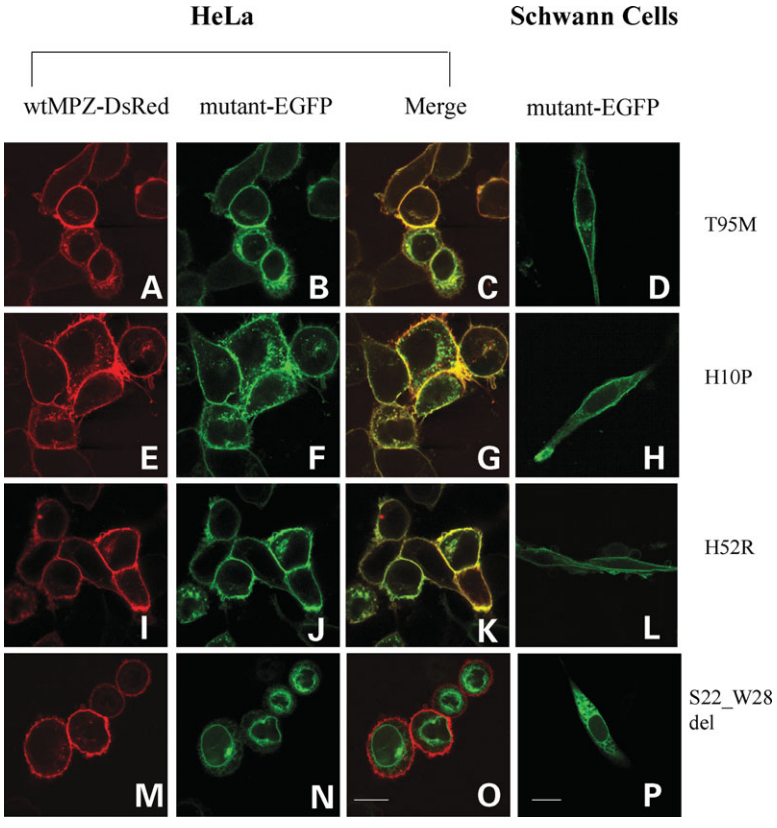

Figure 1. Surface expression on confocal microscope. HeLa cells have been transiently transfected with both wtMPZ-DsRed (**A, E, I, M**) and MPZ mutants conjugated with EGFP (**B, F, J, N**). The third column shows the merging pattern of the two fluorophores (**C, G, K, O**). Both late-onset mutations, T95M (C) and H10P (G) and early-onset H52R (K) co-localized with wtMPZ-DsRed. The early-onset mutation S22_W28del (O) did not co-localize with wtMPZ, but appears to be retained within the cytoplasm. In murine Schwann cells (**D,H,L,P**) the pattern of localization of the mutants-EGFP is comparable with HeLa cells. The late-onset T95M (D) and H10P (H) mutants are clearly trafficked to the membrane surface, as well as the early-onset H52R mutant (L). The S22_W28del early-onset mutation (P) appears to be retained into the cytoplasm of the Schwann cell. Images were collected by confocal microscopy using a MRC-1024 instrument (Bio-Rad, Hercules, CA, USA) attached to a Nikon Diaphot 200 inverted microscope (Nikon Inc., Tokio, Japan) and using a plan-apochromatic oil immersion objective 60×/1.4 numeric aperture. Bars: 14.5 μm.

S22_W28del-EGFP was decreased compared with that of wild-type (0.40 versus 0.75), demonstrating that most of the mutant protein was not reaching the plasma membrane. Thus, the early-onset mutations analyzed have a different pattern of intracellular expression, suggesting a diversity of mechanisms causing early-onset neuropathy.

The pattern of wild-type and mutant MPZ-EGFP expression is similar in HeLa cells and primary Schwann cells

Although HeLa cells have been widely used to study the cellular localization and expression of MPZ and its mutants (12–13), they are not the usual cellular target of MPZ expression. It was thus important to demonstrate that similar patterns of MPZ mutants-EGFP expression and localization also occurred in Schwann cells. Consequently, we transiently transfected primary Schwann cells cultures prepared from murine sciatic nerves with our MPZ-EGFP constructs and analyzed them by confocal microscopy 24 h later. Although, as expected, the transfection efficiency was very low compared with that of HeLa cells, we could analyze at least 20 cells for each mutant. We found that the patterns of MPZ-EGFP localization in Schwann cells were identical to that found in HeLa cells: the late-onset mutants, T95M and H10P and the early-onset mutant H52R were transported to the plasma membrane, while the early-onset mutant S22_W28del was intracellularly retained (Fig. 1). These patterns are thus a consequence of the specific *MPZ* gene mutation.

Late-onset T95M is not glycosylated; early-onset s22_W28del is retained into the cytoplasm and is not trafficked to the trans-Golgi

Glycosylation is a key step in the post-translational processing of MPZ, and occurs at a single site, N93 (1). Most membrane proteins, including MPZ, which undergo this type of N-linked glycosylated are first modified with high mannose carbohydrates within the ER, which are further processed and replaced with low mannose carbohydrates in the Golgi (14). Digestion with endo-H removes high mannose N-linked carbohydrates, whereas digestion with PNGaseF removes all carbohydrates. Endo-H sensitivity thus indicates that a protein has not yet been processed in the trans-Golgi (15). Since wild-type tMPZ undergoes normal N-linked glycosylation in Schwann cells (16), we analyzed the pattern of glycosylation in the

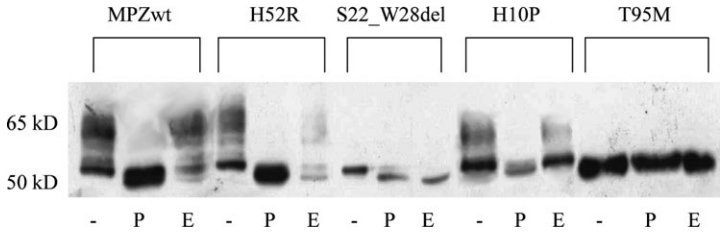

Figure 2. Endoglycosidases digestions. The images show three lanes for each transfected protein corresponding to undigested protein extract (−); proteins digested by PNGaseF (P) and proteins digested with Endo H (E). Undigested proteins ran at 55 kDa (MPZ: 29 kDa; EGFP: 26 kDa), those sensitive to PNGaseF (P) or to endo-H digestion (E) ran at about 51 kDa. Fusion proteins were sensitive to PNGse, except for T95M which was undigestible by both endoglycosidases, demonstrating that this protein is not glycosylated. The S22_W28del was sensitive to endo-H digestion, suggesting that this mutation is retained prior to the trans-Golgi.

four mutant proteins in our study to determine if this pathway was disrupted and could therefore contribute to the neuropathy. As can be seen from our results in Figure 2, all fusion proteins were sensitive to PNGaseF, except for T95M which was indigestible with both endoglicosidases, demonstrating that this protein is not glycosylated and is expressed as an immature protein.

Differently, the early-onset S22_W28del mutant was sensitive to Endo-H, demonstrating that this mutation arrests the aberrant protein prior to arrival in the trans-Golgi (Fig. 2).

Early-onset S22_W28del is retained in the ER

We next performed a series of experiments designed to localize S22_W28del within the cytoplasm, labeling transfected cells for different endocellular compartments, including the ER, the Golgi apparatus and the endosomes. We found that S22_W28del-EGFP co-localized (R_R 0.86) with a specific red fluorescent dye labeling the ER, suggesting that the mutant protein was retained within the ER. Wild-type MPZ-EGFP, as expected, was not retained in the ER (R_R 0.20) (Fig. 3). Immuno-Electron Microscopy (Immuno-EM) also indicated that S22_W28del was retained within the ER. HeLa cells expressing the wtMPZ or the S22_W28del mutation were doubly labeled with an anti-EGFP antibody and an antibody specific for calreticulin, a calcium binding protein, highly expressed in the ER. Co-localization of S22_W28del and calreticulin was clearly visible, while wtMPZ was expressed on the surface and did not co-localize with calreticulin (Fig. 3). None of MPZ mutants nor wtMPZ co-localized with markers for the Golgi compartment and endosomes (data not shown).

S22_W28del causes moderately decreased cellular viability and induces apoptosis but does not activate the unfolded protein response

To determine whether expression of any of the MPZ mutants affected cell viability, we analyzed HeLa cells after transfection using a 3-(4,5-dimethylthiazol-2-yl)-2,5-diphenyltetrazolium bromide (MTT) absorbance assay. Expression of S22_W28del decreased absorbance at 570 nm by 26% compared with control (0.76 ± 0.01, $P < 0.05$), suggesting that cell viability was moderately reduced by expression of this mutation (Fig. 4A). No effects on viability were observed for either of the two late-onset or for the H52R early-onset mutation (T95M: 1.1 ± 0.07; H10P: 0.94 ± 0.01; H52R: 0.96 ± 0.09), when compared with the wild-type protein (1.03 ± 0.003; *P*-value: n.s.), suggesting that expression of these mutations did not alter cell viability.

Similarly, control studies demonstrated that the expression of wtMPZ-EGFP in HeLa cells did not lead to toxic consequences since no differences in terms of cellular viability were observed between wtMPZ transfected cells and those expressing the empty vector pEGFP-N1 (1.03 ± 0.003 versus 1.08 ± 0.003, *P*-value: n.s.).

To investigate further the decreased viability in S22_W28del cells, we determined whether the transfected HeLa cells underwent programmed cell death, or apoptosis. A terminal deoxynucleotidyl Transferase Biotin-dUTP Nick End Labeling (TUNEL) labeling test was performed on cells transfected with wild-type or S22_W28del mutant protein. The number of apoptotic cells was determined by counting TUNEL-positive cells and 4′, 6-diamidino-2-phenylindole (DAPI)-positive nuclei in 10 fields (at least 2000 cells) for each transfection. HeLa cells expressing the S22_W28del protein had significantly greater numbers of apoptotic cells ($5.46\% \pm 0.5$) than those expressing either wild-type protein or vector alone ($1.51\% \pm 0.4$, $P < 0.001$) (Fig. 4B). In contrast, cells exposed to brefeldin A, a compound known to induce apoptosis, had $19.05\% \pm 1.9$ TUNEL-positive cells ($P < 0.0001$) (Fig. 4B). These data thus demonstrate that expression of the mutant protein, S22_W28del, causes a modest but significant increase in programmed cell death, which probably accounts for its effect on cell viability.

Activation of the unfolded protein response (UPR) by misfolded proteins in the ER is one potential cause of apoptosis (17–19). To investigate the UPR in our model we measured Binding Ig Protein (BiP/Grp78) mRNA levels and X-box binding protein 1 (XBP-1) mRNA alternative splicing in S22_W28del and wtMPZ transfected cells. S22_W28del caused increased expression of BiP when compared with wtMPZ cells (3.37 ± 1.7 versus 1.58 ± 0.06), but the difference did not attain significance (Fig. 4C). XBP-1 mRNA alternative splicing was similar for S22_W28del and wild-type cells (0.21 ± 0.08 versus 0.19 ± 0.04, *P*-value: n.s.), (Fig. 4D). Apoptosis can also be induced as part of the UPR, through signaling that involves pancreatic ER kinase

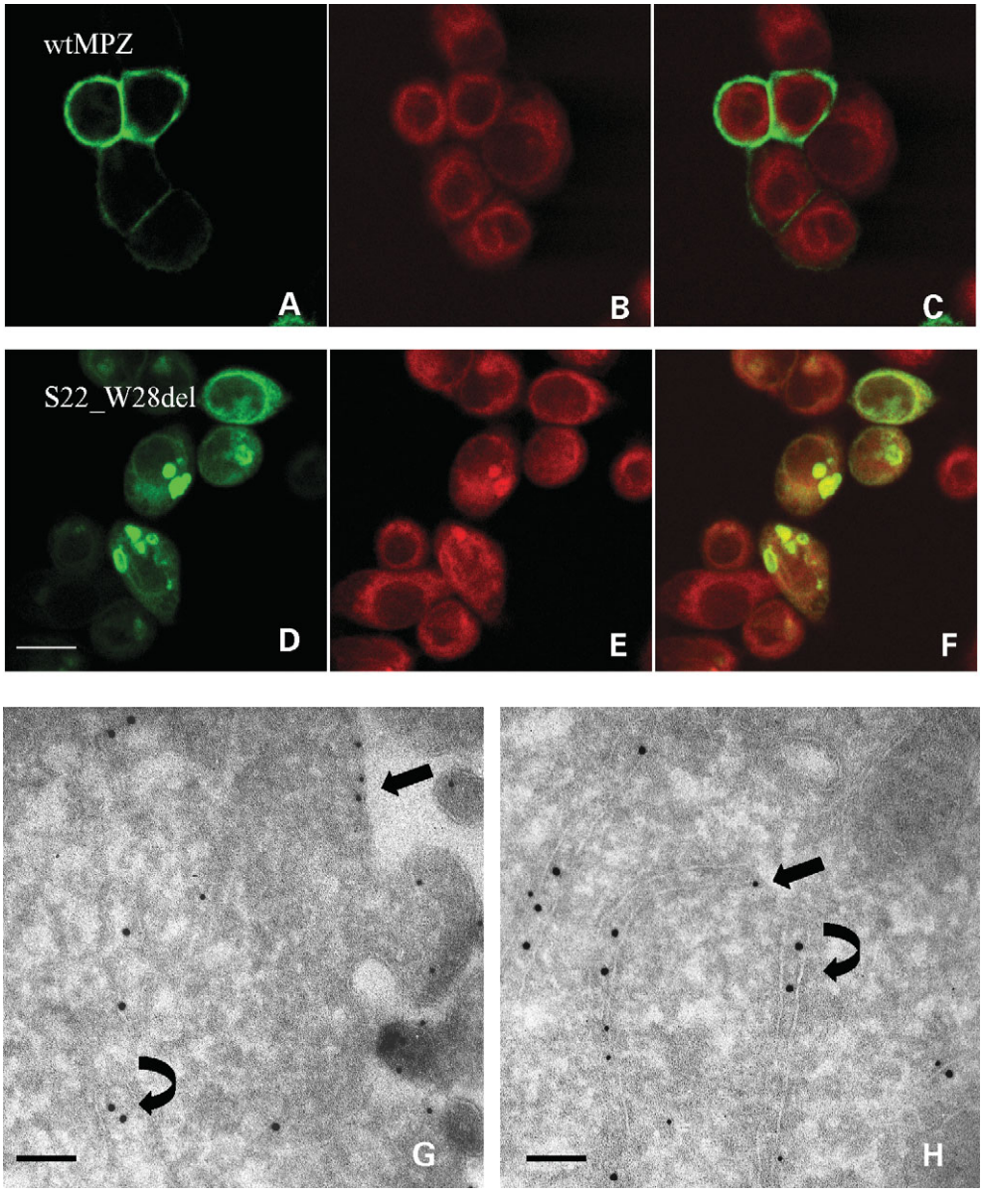

Figure 3. Co-localizazion of S22_W28del with ER markers. HeLa cells were transiently transfected with wtMPZ (**A**–**C**) or S22_W28del (**D**–**F**). After transfection, cells were labeled with the red fluorescent lipophilic tracer: ER-Tracker (Molecular Probes, Invitrogen, Italy, San Giuliano Milanese, MI, Italy) (B and E). The Pearson's correlation coefficient (R_R) between the two fluorences was calculated by evaluating a minimum of 100 cells for each transfection. Wild-type MPZ does not co-localize with the ER-tracer (C), while the mutant S22_W28del (F) co-localizes with the ER marker (R_R 0.86 versus R_R 0.20 of wtMPZ). Bar: 14.5 μm. Immunoelectron microscopy was performed on cells expressing wtMPZ (**G**) and S22_W28del (**H**). EGFP staining was followed by 10 nm colloidal gold-conjugated protein A (straight arrows). The ER was stained by an anti-calreticulin antibody, followed by 15 nm colloidal gold-conjugated protein A (curved arrows). Wild-type MPZ was located on the cellular surface and did not co-localize with calreticulin (G), while the S22_W28del MPZ can be observed in tubular structures which are positive for calreticulin staining (H). Bars: 150 nm.

(PERK) in the ER and the transcription factor CAATT enhancer-binding protein homologous protein (Chop) in the nucleus (17–19). We therefore also measured Chop mRNA levels in the transfected cells. Chop mRNA levels were nearly identical for S22_W28del and wild-type cells (0.55 ± 0.07 versus 0.49 ± 0.11, *P*-value: n.s.) (Fig. 4E). Taken together these data did not support activation of a UPR response in the S22_W28del cells and did not support the UPR as the cause of apoptosis identified in S22_W28del.

Early-onset mutations decrease intercellular adhesion, while late-onset mutations do not interfere with MPZ-mediated aggregation

Early-onset *MPZ* mutations disrupt myelin development, while late-onset mutations permit myelination but subsequently alter axonal–Schwann cell interactions (9–11) leading to axonal degeneration. Since a major role of MPZ is to mediate adhesion between adjacent myelin wraps

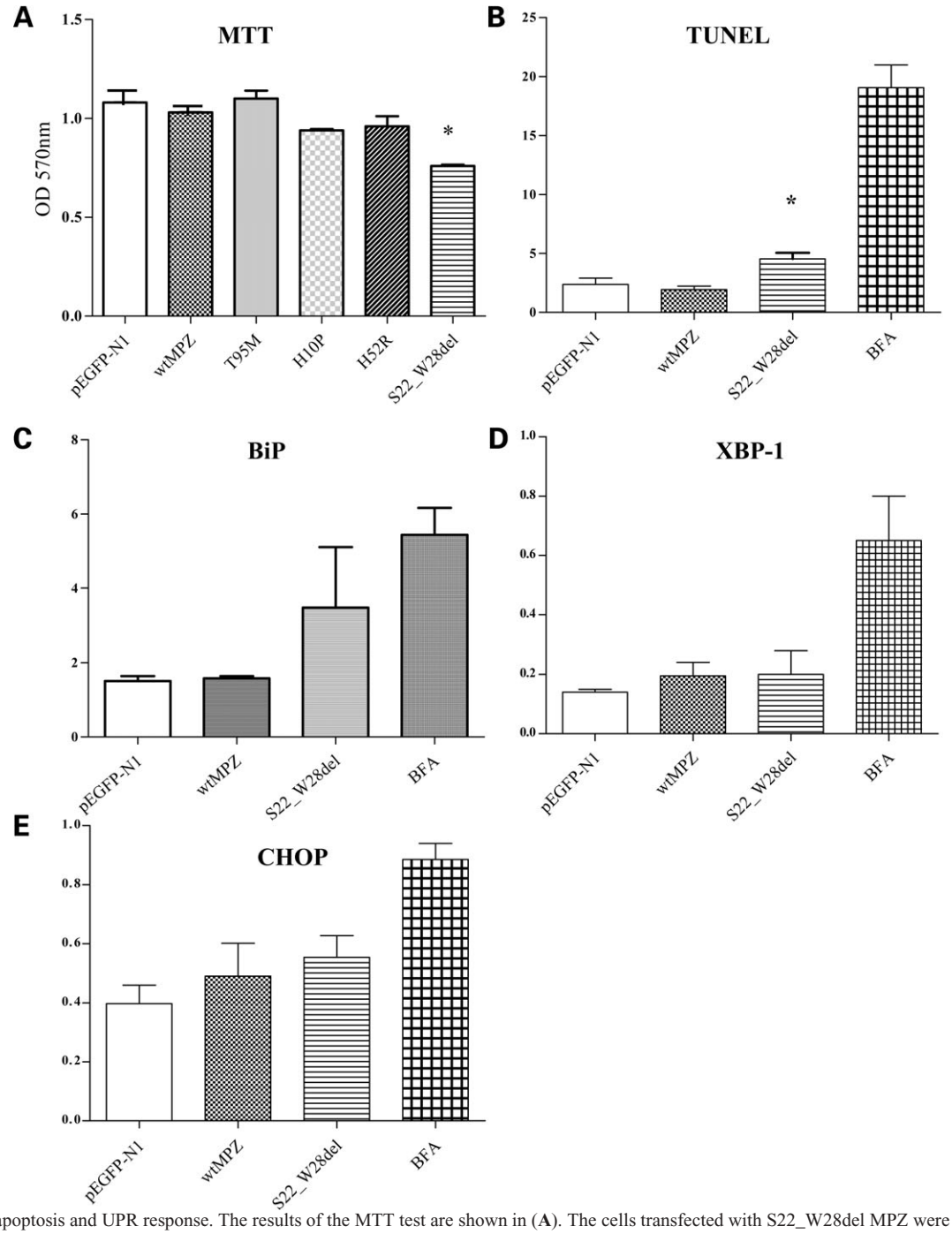

Figure 4. Viability, apoptosis and UPR response. The results of the MTT test are shown in (**A**). The cells transfected with S22_W28del MPZ were characterized by a significantly decreased (*) cellular viability: 0.76 ± 0.01 when compared with cells expressing wtMPZ: 1.03 ± 0.003, $P < 0.05$. The Tunel test (**B**) showed a significantly increased (*) percentage of apoptotic cells in HeLa cells transfected with S22_W28del (5.46% ± 0.5) compared with those expressing the wild-type protein (1.51% ± 0.4, $P < 0.001$). The activation of the UPR was investigated by measuring, by RT–PCR, the expression levels of Bip mRNA (**C**), the XBP-1 mRNA alternative splicing (**D**) and the expression of Chop (**E**). None of those parameters was significantly upregulated in cells expressing the S22_W28del mutation. Cells exposed to BFA represent the positive control.

during myelin development, we hypothesized that early-onset mutations would more significantly disrupt this adhesion process than late-onset ones. To test this hypothesis, we analyzed aggregate formation in HeLa cells transfected with DNA constructs expressing either early or late-onset mutant proteins. In these experiments, we measured the size of the cellular aggregates, which we have previously determined is similar to counting the number of cells within an aggregate, but is much simpler to measure and automate (data not shown). Expression of wild-type protein increased aggregate size compared with untransfected cells in this assay, demonstrating that it was capable of detecting MPZ-mediated adhesion cells expressing either of the two early-onset mutations; formed cellular aggregates that were ∼70%

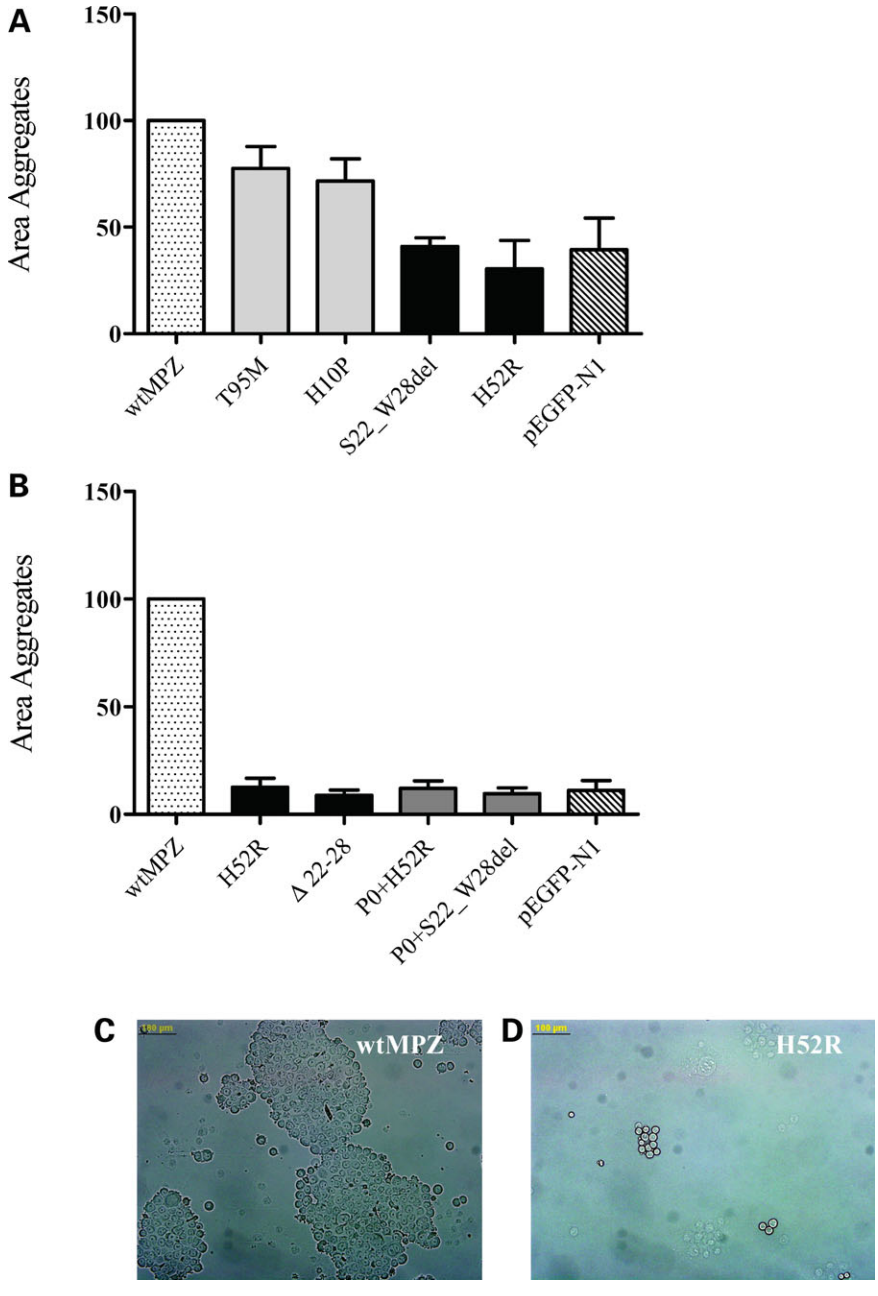

Figure 5. Intercellular adhesion. (**A**) The results of the aggregation test performed with cells transfected with wtMPZ, with each mutant and the empty vector alone (pEGFP-N1). The average surface of aggregates expressing each early-onset mutation, normalized to the area of aggregates produced by wtMPZ expressing cells was reduced to about 30% ($P < 0.001$). The late-onset mutations moderately interfered with intercellular adhesion (*P*-value: n.s.). (**B**) The results of the aggregation test performed on cells expressing wtMPZ, the empty vector alone (pEGFP-N1), the early-onset mutations (H52R, S22_W28del) either alone or doubly transfected with wtMPZ. The average surface of aggregates formed by cotransfected cells was comparable (*P*-value: n.s.) with those observed from cells expressing the mutation alone. These data suggest that both early-onset mutations prevent the correct function of the wild-type protein. (**C**) Example of aggregate formed by wtMPZ expressing cells. (**D**) Example of aggregate formed by H52R transfected cells. Bars: 100 μm.

smaller (Fig. 5D) than those expressing wild-type protein (Fig. 5C), suggesting that these proteins had a significant effect on the MPZ-mediated adhesion process (H52R: 0.27 $\pm$ 0.12; S22_W28del: 0.32 $\pm$ 0.12), similar to the empty vector transfected cells (0.22 $\pm$ 0.01), ($P < 0.001$) (Fig. 5A). In contrast, expression of the late-onset mutations reduced aggregate size by only 30%, suggesting these proteins had less of an affect on adhesion (T95M: 0.78 $\pm$ 0.15; H10P: 0.72 $\pm$ 0.15, *P*-value: n.s.) (Fig. 5A).

Since *MPZ* mutations cause neuropathy in the heterozygous state, co-expression of wild-type and mutant protein could alter the results obtained by expression of mutant protein alone. To investigate this possibility, we repeated the cell aggregation in HeLa cells co-transfected with constructs

expressing both an early-onset and wild-type protein. In these experiments, aggregate formation was again reduced to ~70%, similar to the results in singly transfected cells (H52R: 0.23 ± 0.01; H52*R*+wtMPZ-DsRed: 0.34 ± 0.04; S22_W28del: 0.22 ± 0.04; S22_W28del+ wtMPZDsRed: 0.22 ± 0.01). Co-expression of both fluorescently tagged wild-type proteins, however, did not significantly alter aggregate size (0.98 ± 0.3), demonstrating that the tagged sequences did not affect the experimental outcome. Thus expression of early-onset mutations not only disrupts adhesion themselves, but they also prevent adhesion of the wild-type protein expressed from the normal allele. Taken together, these data show that early-onset mutations have a more significant effect on MPZ-mediated adhesion than do late-onset mutations, suggesting there is a relationship between alteration of adhesion and disease severity.

Previous studies (20) have shown that N-cadherin expression is upregulated in HeLa cells stably transfected with wtMPZ, which may contribute to intercellular adhesion. To investigate this point we evaluated N-cadherin (*CDH2)* mRNA expression by quantitative real-time RT–PCR (qRT–PCR) in HeLa cells transiently transfected with wild-type MPZ-EGFP and MPZ-EGFP mutants. In most of these experiments, however, expression of wild-type or mutant MPZ did not induce the expression of the *CDH2* gene (wtMPZ: 1.21 ± 0.04; T95M: 0.92 ± 0.02; H10P: 1.73 ± 0.36; S22_W28del: 1.34 ± 0.35) compared with that of HeLa cells transfected with p-EGFP-N1 (1.12 ± 0.17, *P*-value: n.s.). N-cadherin expression is therefore not responsible for the increased aggregation properties observed in the presence of wtMPZ.

The relative expression of *CDH2* was approximately 3-fold higher (3.67 ± 0.19) in cells transfected with H52R mutant compared with cells expressing the empty vector (1.12 ± 0.17) alone, $P < 0.05$. We cannot explain why the mutation H52R caused a moderate upregulation of N-cadherin, however this does not seem to counterbalance the decreased adhesion caused by this mutant.

DISCUSSION

CMT1B is caused by mutation in one of at least 100 different amino acids within *MPZ*. Although the etiology of the disease is heterogeneous, there are two main clinical phenotypes produced by *MPZ* mutations: one with early-onset of symptoms, delayed motor milestones and very slow conduction velocities; and a second with adult onset of symptoms and essentially normal NCV. In our current work reported here, we have begun to investigate the molecular mechanisms underlying these phenotypes by analyzing the effect of expression of mutant proteins in heterologous cells. Interestingly, these studies demonstrate that the two CMT1B phenotypes are caused by at least three different molecular mechanisms.

The mutants T95M and H10P, both of which cause a late-onset neuropathy, are normally trafficked to the plasma membrane and moderately affect intercellular adhesion. Based on our data, normal trafficking and a moderate decrease of intercellular adhesion could be necessary components of late-onset mutations and support a partial loss of function, as possible pathomechanism. However, neither normal trafficking nor normal or mildly decreased adhesion are sufficient by themselves to accurately predict early or late-onset disease. Previous studies have shown that the cytoplasmic mutation R198S MPZ is transported normally to the plasma membrane, abolishes adhesion, but ultimately causes a late-onset neuropathy, presumably by altering signal transduction pathways involving the RSTK domain between amino acids 198S and K201 (7). Ultimately, whether a particular heterozygous MPZ mutation causes a late-onset neuropathy appears to depend as much on interactions between the mutant and wild-type protein as on whether the mutant protein can be transported to the myelin sheath.

Interestingly, we have shown that N93 is not glycosylated in late-onset T95M, consistent with the fact that the glycosylation motif (N-X-S/T), necessary for asparagine glycosylation is altered (14). The glycosylation of MPZ consists of the addition of a single oligosaccharide, N-linked to N93 in the extracellular domain (1). This oligosaccharide is complex, sulfated (21) and contains the HNK-1 moiety, also found in PMP-22 and myelin-associated glycoprotein (MAG) (22). The function of this MPZ oligosaccharide is not understood in detail but N93 has been shown to be necessary for intercellular adhesion in CHO cells (23–24). Despite the importance of glycosylation for MPZ function, mutations preventing MPZ glycosylation do not appear to delay PNS myelination, and do not by themselves cause early-onset neuropathy, at least when the mutations are in the heterozygous state. Thus, T95M which completely prevents MPZ glycosylation only causes a late-onset neuropathy with minimal demyelination (25). Additionally, a heterozygous N93S mutation has been reported to cause a late-onset neuropathy (26).

The HNK-1 epitope, expressed by different glycolipids and glycoproteins sharing adhesion properties, like N-CAM and L1, appear to be involved in astrocyte–astrocyte, neuron–astrocyte and neural cell–substrate interactions (27). It is conceivable, that L2/HNK-1 epitope could be part of the heterophilic interaction of P0 (27) with peripheral nervous axons. In this framework, the loss of the normal glycosylation pattern of T95M, is of particular interest and could affect the axonal–glia interactions.Taken together these results demonstrate that reduced glycosylation does not impair PNS myelination. Rather the mutations disrupt at least in part glial–axonal interactions so that axonal degeneration ultimately occurs with at most mild evidence of segmental demyelination.

Early-onset mutations appear to cause neuropathy by at least two distinct processes, only one of which involves impaired intracellular trafficking.

Our observation on S22_W28del transfected cells, including the co-localization with both the ER fluorescent dye and the anti-calreticulin antibody, together with the sensitivity to Endo H digestion, all suggest that this missence change leads to a prevalent retention of the mutated protein into the ER. However, impaired trafficking of the mutant protein by itself, cannot explain the early-onset phenotype. For example MPZ +/− mice have a 50% reduction of MPZ in myelin, which would be similar to having protein from one allele retained in the ER, and these animals develop only a mild, late-onset neuropathy (28–29). Additional mechanisms,

including decreased cell viability and increased apoptosis, may result in an abnormal gain of function phenotype that recalls the more severely affected homozygous MPZ −/− mouse (30). Interestingly, the protein did not activate the UPR, while another MPZ mutant, the deletion of serine 34 (S34del; or S63del including the signal peptide) was both retained within the ER of transgenic Schwann cells and induced CHOP and BiP, suggesting activation of the UPR (31). The reasons for the difference in UPR activation by the two mutants proteins are not clear. In Trembler J (Tr^J) mice, caused by a missense mutation in the *PMP22* gene, the mutant protein is retained in the ER with no detectable activation of BiP and CHOP expression (32), similar to our findings. In those animals, a proteasomal inability to eliminate the cytoplasmic inclusions of the mutated PMP22 protein was suggested as contributing to the pathogenesis of Tr^J neuropathy (33). Whether a proteasomal impairment or an increased Schwann cell turnover also contribute to the pathogenesis of S22_W28del remains to be demonstrated, perhaps in knockin animal models of the mutation.

Alternatively, H52R mutations appear to cause early-onset neuropathy by a distinct mechanism. In this case the mutant protein is normally transported to the cell surface where it causes neuropathy by 'dominant negative' effects that alter the structure of myelin to the extent that normal myelination is prevented or the maintenance of functional myelination is impaired. Exactly how this occurs is unknown but may be related to the fact that the histidine at amino acid 52 has been shown to be a critical amino acid for the adhesive interface of MPZ, based on the crystal structure of the MPZ extracellular domain (5). Arginine, which lacks the histidine ring structure, may alter the adhesive interface of tetramers formed from both wild-type and mutant protein to disrupt the process of myelination. Consistent with this notion, mice expressing the S34C mutation, causing early-onset CMT1B in patients, have compact myelin which likely incorporates the mutant protein, but in which myelin packing is abnormal compared with wild-type animals (34).

In summary, we have shown that early and late-onset CMT1B are likely to be caused by multiple pathogenic mechanisms involving gain of function, dominant negative effects and partial loss of function. Additional mechanisms such as nonsense-mediated decay from mutations that prematurely truncate the mRNA (13), producing haploinsufficiency, as observed in MPZ +/− mice may also play a role in specific cases. Determining the mechanisms by which these mutations cause neuropathy will provide insights into molecular pathways involved in demyelination and provide a rational basis for the treatment of early and late-onset CMT1B.

MATERIAL AND METHODS

HeLa cells culture

HeLa cell line were maintained in Dulbecco's Modified Eagle's Medium supplemented with 10% heat inactivated fetal bovine serum, 2 mM L-glutamine and 50 units/ml penicillin and 50 μg/ml streptomycin at 37°C, in a humidified incubator with 5% CO_2. All media and supplements for cellular cultures were purchased from Gibco (Invitrogen, Italy, San Giuliano Milanese, MI, Italy).

Primary Schwann cells cultures

Sciatic nerves were sterilely isolated from 3-week-old FVB/N wild-type mice [Charles River Laboratories Italia S.r.l, Calco (Lecco) Italy], housed in specific pathogen-free conditions. Nerves were pooled (six–eight mice per experiment), minced into small pieces and transferred to Leibovitz L-15 Medium containing 0.125% collagenase and 8 U/ml Dispase, for 2 h at 37°C on a rocking table. The cell suspension was centrifuged at 1400 rpm (Swing-bucket rotor A-4–44 Eppendorf S.r.l Italian Branch, Milan, Italy), filtered through a 40 μm cell strainer (BD Italia, Buccinasco, Milan, Italy) and seeded on a 35 mM dish coated with CellBIND® Surface (Corning Incorporated Life Sciences, Lowell, MA, USA). Cultures were incubated at 37°C, 5% CO2 in serum-free N2HRG culture medium (35), composed of a 1:1 ratio of DMEM and F-12 supplemented with 0.5 ng/ml Na-selenite (Sigma-Aldrich S.r.l., Milan, Italy), 1.6 μg/ml putrescine (Sigma-Aldrich S.r.l., Milan, Italy), 0.63 ng/ml progesterone (Sigma-Aldrich S.r.l., Milan, Italy), 0.1 mg/ml transferrin (Sigma-Aldrich S.r.l., Milan, Italy), 0.5 μg/ml insulin (Sigma-Aldrich S.r.l., Milan, Italy), gentamycin (50 μg/ml), fungizone (2.5 μg/ml), 2 μM forskolin (Sigma-Aldrich S.r.l., Milan, Italy), 10 ng/ml neuregulin 1 (R&D Systems, Minneapolis, MN, USA). Twenty-four hours after plating, the medium was replaced with fresh one and nonadhesive cells were discarded. After 4 days, cells were trypsinized, counted and 50 000 cells per well were seeded on a chamber slide (Nalge Nunc International, Rochester, NY, USA), previously coated with mouse laminin (10 mg/ml) (Sigma-Aldrich S.r.l., Milan, Italy). If not otherwise specified, all media and supplements for cellular cultures were purchased from Gibco (Invitrogen, Italy, San Giuliano Milanese, MI, Italy).

Most of the cells were small, spindle shaped, displaying the classical morphology of cultured Schwann cells, but some underlying fibroblasts with a large flattened shape, resembling a 'fried egg', were also observed. The average percentage of fibroblasts was calculated in three independent primary Schwann cultures, after 4 days of culture. Using an inverted microscope (model IB2, EXACTA+OPTECH Labcenter S.p.a, S. Prospero, Modena, Italy) equipped with a digital camera (Canon Power Shot A640), 20 frames, including at least 1000 cells, were randomly digitalized at 40× magnification and analyzed using the Pro Plus Imaging System (Immagini e Computer, Rho, Italy). The percentage of fibroblasts, based on morphological evaluation, was calculated for each image and ranged from 1.7 to 3.5%, thus meaning that, at this time point, our Schwann cells cultures were >95% pure.

Plasmids and site-directed mutagenesis

The full-length human cDNA of wild-type *MPZ* gene (kindly provided by K. Hayasaka) was cloned into the plasmid pBlue-Script® II SK(−) Phagemid Vector (Stratagene, La Jolla, CA, USA). Human *MPZ* mutations were introduced by site-direct mutagenesis (QuikChange Site-Directed Mutagenesis Kit,

Stratagene, La Jolla, CA, USA), using specific primers containing the nucleotide changes according to manufacturer's protocol. The mutated cDNAs were amplified by PCR using primers containing restriction enzyme sites for *Eco*RI and *Bam*HI, and then fused in-frame into the expression vectors for mammalian cells pEGFP–N1 (Clontech, Mountain View, CA, USA). EGFP was converted to a monomeric form, by introducing the mutation A207K (36), to prevent the chance of erroneous intracellular retention, due to dimerization. All constructs were purified and verified by automated fluorescent sequence analysis (DNA sequencing facility, Wayne State University, Detroit, MI, USA). The human cDNA coding for the human wild-type MPZ was also cloned into another expression vector: pDsRed-Monomer-N1 (Clontech, Mountain View, CA, USA) in frame with DsRed. We selected those vectors in order to produce fusion proteins to the N-terminus of MPZ, reasoning that an intracellular tag would have a minor impact on intercellular adhesion.

Transient transfection

HeLa cells were transiently transfected with each mutant-EGFP construct, by single transfection or in cotransfection with wild-type MPZ-DsRed, using Lipofectamine 2000 (Invitrogen, Italy, San Giuliano Milanese, MI, Italy), according to manufacturer's instructions. The transfection efficiency with all constructs, measured by flow cytometry (FACS Canto, Becton Dickinson Italia S.p.A., MI, Italia), ranged from 62 to 70%.

Primary Schwann cells, previously seeded on a chamber slide (Nalge Nunc International, Rochester, NY, USA), coated with mouse laminin, were transfected using Lipofectamine 2000, similarly to HeLa cells. The percentage of transfected cells was extremely low compared with HeLa cells. To measure the percentage of transfection, a 4′, 6-diamidino-2-phenylindole (DAPI) staining (Molecular Probes, Invitrogen, Italy, San Giuliano Milanese, MI, Italy) was performed according to supplier's recommendations. The average percentage of EGFP-positive cells and DAPI-positive nuclei in 10 sections (at least 1000 cells for each transfection) was calculated and it was quantified as ranging from 0.5 to 2% of Schwann cells.

Confocal microscopy

Surface expression. To study the surface expression of wtMPZ and each mutation, HeLa cells were transiently transfected both with wtMPZ-DsRed and MPZ mutants-EGFP, grown for 24 h in chamber slides (Nalge Nunc International, Rochester, NY, USA) and fixed in 4% parafolmaldehyde for 10 min. Primary Schwann cells were transfected with MPZ mutants-EGFP, grown for 24 h in chamber slides (Nalge Nunc International, Rochester, NY, USA) and fixed in 4% parafolmaldehyde for 10 min.

Intracellular trafficking. The intracellular trafficking of the mutant proteins conjugated with EGFP was investigated using the red fluorescent lipophilic tracers: ER-Tracker and TexasRed-conjugated Wheat Germ Agglutinin (Molecular Probes, Invitrogen, Italy, San Giuliano Milanese, MI, Italy), labeling the ER and the Golgi apparatus, respectively. After transfection with mutants-EGFP, HeLa cells were grown for 24 h in chamber slides (Nalge Nunc International, Hereford, UK) and fixed in 4% parafolmaldehyde for 10 min. The tracer molecules were added to the chamber slides, 30 min before imaging, according to manufacturer's instructions.

Endosomes were labeled with a rabbit polyclonal antibody directed against Early Endosomal Antigen 1 (EEA1 antibody, Cell Signaling Technology Inc, Danvers, MA, USA) according to manufacturer's instructions, followed by a goat anti-rabbit conjugated to Alexa Fluor 568 antibody (Invitrogen, Italy, San Giuliano Milanese, MI, Italy).

For both surface expression and intracellular trafficking experiments, images were collected by confocal microscopy using an MRC–1024 instrument (Bio-Rad, Hercules, CA, USA) attached to a Nikon Diaphot 200 inverted microscope (Nikon Inc., Tokyo, Japan) and using a plan-apochromatic oil immersion objective $60\times/1.4$ numeric aperture. For HeLa cells at least 20 randomly selected frames, including a minimum of 100 cells, were evaluated for each condition. For Schwann cells, due to the low transfection efficiency, we acquired 20 cells for each transfection experiment. The excitation/emission wavelengths were 488/522 for EGFP and 567/605 for DsRed/ER-Tracker/TexasRed-conjugated Wheat Germ Agglutinin/goat anti-rabbit conjugated to Alexa fluor 568. For each excitation wavelength, the laser power was adjusted as necessary to utilize the full dynamic range of the detector and sequential acquisitions were performed to avoid 'cross-talk' between color channels. Series of 8-bit greyscale images (z-series), 512×512 pixel in size were collected at increments of 0.3 μm.

The confocal image files of HeLa cells doubly transfected with MPZ mutant-EGFP and wtMPZ-DsREd were further processed, using the Image J 1.34f software (National Institute of Health, Bethesda, MD, USA), to calculate the Pearson's correlation coefficient (R_R). We reported, for each transfection, the average R_R value corresponding to a minimum of 100 cells.

Immuno-electron microscopy

HeLa cells transfected, with mutants-EGFP or doubly transfected with mutants-EGFP and wtMPZ-DsRed, were fixed for 2 h, at RT, in 2% paraformaldehyde/0.2% glutaraldehyde in PBS, washed with PBS containing 0.02 M glycine, scraped off, centrifuged at 10 000 rpm (rotor A-8-11, Eppendorf S.r.l Italian Branch, Milan, Italy) and embedded in 12% gelatin in PBS. Embedded cells were incubated overnight, on a rocking table, with 2.3 M sucrose at 4°C, mounted on aluminum pins and snapfrozen in liquid nitrogen. Ultrathin cryosections of 60 nm were collected on Formvar-coated copper grids. After blocking unspecific antigenic sites, sections were incubated with a rabbit anti-EGFP antibody (Molecular Probes, Invitrogen, Italy, San Giuliano Milanese, MI, Italy), diluted 1:50 in blocking solution for 30′ followed by 10 nm colloidal gold-conjugated protein A (from G. Posthuma, Department of Cell Biology, Institute of Biomembranes, University Medical Centre Utrecht, The Netherlands) at RT for 30′. After a first fixation in 1% glutaraldehyde, a rabbit antibody anti-calreticulin (Abcam, Cambridge, UK) diluted 1:1000 in blocking solution, was applied and followed by 15 nm colloidal

gold-conjugated protein A (from G. Posthuma, Department of Cell Biology, Institute of Biomembranes, University Medical Centre Utrecht, The Netherlands) at RT for 30′. Finally, sections were fixed with the same procedure already described, then post-stained in 4% neutral uranyle acetate, embedded in 1.25% methyl cellulose and observed with use of an electron microscope (Zeiss EM109, Carl Zeiss S.p.A Italia, Milano, Italy) at 80 kV.

All chemicals, if not specified, are from Sigma-Aldrich S.r.l., Milan, Italy.

Biotinylation assay

Transiently transfected cells (wtMPZ-EGFP and mutants-EGFP) were treated with sulfosuccinimido-NHS-biotin (1.5 mg/ml; Pierce, Rockford, IL, USA) at 4°C for 1 h in PBS/Ca–Mg (37). Biotinylating reagents were removed by washing with 100 mM glycine in PBS/Ca–Mg twice and by further quenching with 100 mM glycine for 30 min, and then cells were lysed with radioimmunoprecipitation assay buffer (RIPA). Supernatants were incubated with streptavidin magnetic beads (2 mg of beads/500 μl of supernatant; New England Biolabs, Ipswich, MA, USA) for 1 h at RT. Beads were washed three times with RIPA buffer, and adsorbed proteins were eluted with 100 μl of Laemmli loading buffer. Then 10 μl of total cell lysate, 10 μl of lysate after incubation with streptavidin beads, 20 μl of the last wash and the bead eluate (10 μl) were separated by SDS–PAGE (8%) and immunoblotted with rabbit anti-EGFP antibody (1: 2500, Molecular Probes, Invitrogen, Italy, San Giuliano Milanese, MI, Italy) and with anti-rabbit HRP-conjugated secondary antibody (1:5000 goat, Amersham, GE Healthcare Europe GmbH—Italian Branch, Milano, Italy). Immunoreactive bands were visualized by ECL on hypersensitive ECL film (Amersham, GE Healthcare Europe GmbH—Italian Branch, Milano, Italy), and scanned bands were quantitated with Image J software (National Institute of Health, Bethesda, MD, USA). Values of MPZ-EGFP surface protein were normalized by levels of MPZ in total cell extracts (ratio surface MPZ-EGFP/total MPZ-EGFP).

Endoglycosidase digestions of membrane proteins

Total proteins were extracted with RIPA buffer and aliquots (10 μl) from the total protein eluate were digested with either Endoglycosidase H (Endo–H) (Roche Applied Science, Monza, Italy) or peptide *N*-glycosidase-F (PNGaseF), (New England Biolabs, Ipswich, MA, USA). Both endoglycosidase digestions were performed for 3 h at 37°C. Endo-H digestions were performed in 50 mM sodium acetate, pH 5.5, with 0.2 units/ml endo-H. PNGaseF digestions were performed with 0.2 units/ml in 5× digestion buffer and 1.25% Igepal. Undigested cell lysates and those digested with endo-H or PNGaseF were separated by SDS–PAGE (8%) and immunoblotted and immunoblotted with rabbit anti-EGFP antibody (1: 2500, Molecular Probes, Invitrogen, Italy, San Giuliano Milanese, MI, Italy) and with anti-rabbit HRP-conjugated secondary antibody (1:5000 goat, Amersham, GE Healthcare Europe GmbH—Italian Branch, Milano, Italy).

Cell toxicity test

A colorimetric assay, based on the cleavage of the yellow tetrazolium salt MTT to purple formazan crystals by dehydrogenase activity in active mitochondria, was used to assess wtMPZ and mutants-mediated toxicity. After transfection, HeLa cells were incubated with the MTT solution (Sigma-Aldrich S.r.l., Milan, Italy) at the final concentration 0.5 mg/ml for 3 h. Formazan crystal, formed in living and metabolically active cells, were then solubilized by adding a 10% SDS in 0.01 M HCl solution to the cells. The number of living cells correlated with the amount of purple formazan crystals, as measured by the absorbance at 570 nm. Given the variability of this test, 30 independent transfections were examined. A unpaired *t*-test was used to compare the empty vector and each mutation to the wtMPZ. The difference was considered significant if $P < 0.05$.

Semiquantitative RT–PCR for UPR-related genes

First-strand cDNA synthesis and semiquantitative amplification were performed by co-amplification of the gene of interest, together with 18S ribosomal RNA, as internal control (Primers: 5′GGGGCCCGAAGCGTTTACT 3′; 5′ GGTCGGAACTACGACGGTTATC 3′). Preliminary experiments ensured that the quantitation was done in the exponential phase of the amplification process and that expression of the reference gene was uniform. Results were expressed as a ratio between the gene of interest intensity band and the intensity of the 18S rRNA band, as measured on the Gel Doc 1000 image system (Bio-Rad, Hercules, CA, USA). For each mutation, experiments were repeated for three times starting from different transfections. Statistical analysis was performed by means of Student's *t*-test for unpaired data, comparing wild-type and MPZ mutants. Statistical significance was defined as $P < 0.05$.

Each set of experiments included HeLa cells transfected with MPZ mutations, HeLa cells transfected with wtMPZ-EGFP, HeLa cells transfected with the empty vector, untransfected HeLa cells and, as positive control, untransfected HeLa cells treated for 24 h with brefeldin A (1 μg/ml; Calbiochem, San Diego, CA, USA). RNA extraction was performed 24 h after transfection using TriZol Reagent (Invitrogen, Italy, San Giuliano Milanese, MI, Italy). PCR reaction was performed by co-amplification of the BiP gene, using primers corresponding to exon 6 (5′-TAGCGTATGGT GCTGCTGTC-3′) and exon 8 (5′- TTTGTCAGGGGTC TTTCACC-3′) or Chop gene, using primers corresponding to exon 3 (5′-TGGAAGCCTGGTATGAGGAC-3′) and exon 4 (5′- TGTGACCTCTGCTGGTTCTG-3′), with 18S rRNA, as already described. Quantification of XBP-1 alternative splicing was performed according to published protocol (19). Digestion products were analyzed on 2% agarose gels, and band intensity was measured as described.

Quantitative estimation of N-cadherin mRNA by real-time RT–PCR

HeLa cells were transiently transfected with wtMPZ, pEGFP-N1 alone and with all MPZ mutants as described

earlier. From each transfectant total RNA was extracted with the RNeasy Mini Kit (Qiagen S.p.A., Milano, Italy) and 1 μg of the DNase-treated RNA was reverse transcribed into cDNA by incubating it at 42°C for 1 h with 20 pmol of oligo(dT), 500 μM dNTPs, 30 U of RNase inhibitor (Eppendorf, Milan, Italy) and 200 U Moloney murine leukemia virus reverse transcriptase in a total volume of 20 μl (all reagents, if not otherwise specified are from Invitrogen, Italy, San Giuliano Milanese, MI, Italy). Intron-spanning primers for N-cadherin (*CDH2)*, corresponding to exon 13 (5′-CACCGGTGCCATCA TTGC-3′) and exon 14 (5′-GGCCTGGCGTTCTTTATCC-3′) and a TaqMan MGB probe (5′-YAK- CCATACCACAAA CATCAGCACAAG-BBQ-3′) were designed. Quantification of N-cadherin mRNA expression was performed on a Rotor-Gene 3000 instrument (Corbett Life Science, Sydney, Australia). The thermal cycler parameters were as follows: 10′ at 95°C for one cycle followed by amplification of cDNA for 40 cycles with melting for 30″ at 95°C and annealing and extension for 50″ at 60°C.

Two independent experiments, with samples run in triplicate, were performed. As endogenous control Polymerase II polypeptide A (*POLR2A*) was co-amplified in the reaction using a FAM labeled probe. Running the PCR without cDNA (negative control) yielded no detectable product. The amount of fluorescence accumulated exponentially after 28 cycles of reaction in all tubes. The relative expression of *CDH2* among the samples was calculated using the ΔΔCt method as implemented in the Rotorgene 3000 software (Corbett Life Science, Sydney, Australia). *CDH2* expression was normalized among samples using the *POLR2A* expression level and was represented as fold of pEGFP-N1 expression, by arbitrarily setting at 1 the first of the three replicate samples containing cDNA from HeLa cells expressing the empty vector alone. A one-way analysis of variance followed by a Bonferroni post-test was used to analyse the experiment. The difference was considered significant if $P < 0.05$.

Tunel test

Labeling of DNA strand breaks by terminal deoxynucleotidyl transferase (TdT) was assessed, using an *in situ* cell death detection kit, TMR red (Roche Applied Science, Monza, Italy). Cells were grown in chamber slides (Nalge Nunc International, Rochester, NY, USA), transiently transfected and allowed to recover 30 h in complete medium without antibiotics. Cells were then fixed with 4% paraformaldehyde in PBS at room temperature for 10′, washed with PBS and permeabilized with 0.1% Triton X-100 in PBS on ice for 2′. TUNEL staining was performed according to supplier's recommendations, for 1 h at 37°C, in the dark. The average percentage of TUNEL-positive cells and DAPI-positive nuclei in 10 sections (at least 2000 cells for each transfection) was calculated. Student's *t* tests for unpaired data, comparing wild-type and MPZ mutants were performed. Statistical significance was defined as $P < 0.05$.

Intercellular adhesion

The aggregation test was performed, based on the method described by Filbin *et al*. (2), with personal modifications. After 24 h from transient transfection, cells were washed with PBS and incubated with 0.25% trypsin in PBS for 3 min at RT, counted in Bürker chambers and resuspended to a final concentration of 1.5×10^6 cells/ml in DMEM containing 10%FCS and 25 mM of Hepes to maintain the cellular pH. By three passages through an 18-gauge syringe, we obtained a single cell suspension. Suspensions, containing a minimum of 95% single cells, were allowed to aggregate at 37°C with gentle rocking at 5 rpm. After 3 h, the tubes were gently inverted and aliquots of 10 μl were removed, put on a microscope slide and covered with a 21 × 26 mM cover slip, without using fixatives and immediately examined under the microscope (Olympus AX60, Olympus Italia S.r.l., Milano, Italy). From each slide, 30 frames, randomly selected at 20× magnification, were digitalized and stored, using the Pro Plus Imaging System (Immagini e Computer, Rho, MI, Italy). The area of cellular aggregates (>5 cells) were measured with Pro Plus Imaging System (Immagini e Computer, Rho, MI, Italy) and the average area of aggregates formed by HeLa cells transfected with each mutant was calculated and normalized to the average area of aggregates produced by wtMPZ expressing cells. An unpaired *t*-test was applied, comparing each mutant to the wild-type protein. The difference was considered significant if $P < 0.05$.

ACKNOWLEDGEMENTS

We thank Janne Balsamo and Jack Lilien for kindly sharing with us their experience and thoughts on Myelin Protein Zero and on intercellular adhesion assays. We are grateful to Fabio Ghiotto for designing the qRT–PCR experiments.

Conflict of Interest statement. None declared.

FUNDING

The financial supports of PRIN (2005060584_004), Telethon GGP06178 and GUP05007 to A.S. are gratefully acknowledged.

REFERENCES

1. Lemke, G. and Axel, R. (1985) Isolation and sequence of a cDNA encoding the major structural protein of peripheral myelin. *Cell*, **40**, 501–508.
2. Filbin, M.T., Walsh, F.S., Trapp, B.D., Pizzey, J.A. and Tennekoon, G.I. (1990) Role of myelin P0 protein as a homophilic adhesion molecule. *Nature*, **344**, 871–872.
3. Spiryda, L.B. (1998) Myelin protein zero and membrane adhesion. *J. Neurosci. Res.*, **54**, 137–146.
4. Eichberg, J. (2002) Myelin P0: new knowledge and new roles. *Neurochem. Res.*, **27**, 1331–1340.
5. Shapiro, L., Doyle, J.P., Hensley, P., Colman, D.R. and Hendrickson, W.A. (1996) Crystal structure of the extracellular domain from P0, the major structural protein of peripheral nerve myelin. *Neuron*, **17**, 435–449.
6. Wong, M.H. and Filbin, M.T. (1994) The cytoplasmic domain of the myelin P0 protein influences the adhesive interactions of its extracellular domain. *J. Cell Biol.*, **126**, 1089–1097.
7. Xu, W., Shy, M.E., Kamholz, J., Elferink, L., Xu, G., Lilien, J. and Balsamo, J. (2001) Mutations in the cytoplasmic domain of P0 reveal a role for PKC−mediated phosphorylation in adhesion and myelination. *J. Cell Biol.*, **155**, 439–446.

8. Gaboreanu, A.M., Hrstka, R., Xu, W., Shy, M., Kamholz, J., Lilien, J. and Balsamo, J. (2007) Myelin protein zero/P0 phosphorylation and function require an adaptor protein linking it to RACK1 and PKC{alpha}. *J. Cell Biol.*, **177**, 707–716.
9. Shy, M.E., Jani, A., Krajewski, K., Grandis, M., Lewis, R.A., Li, J., Shy, R.R., Balsamo, J., Lilien, J., Garbern, J.Y. and Kamholz, J. (2004) Phenotypic clustering in MPZ mutations. *Brain*, **127**, 371–384.
10. Bai, I., Ianokova, E., Pu, Q., Ghandour, K., Levinson, R., Martin, J.J., Ceuterick-de Groote, C., Mazanec, R., Seeman, P., Shy, M.E. and Li, J. (2006) Effect of an R69C mutation in the myelin protein zero gene on myelination and ion channel subtypes. *Arch. Neurol.*, **63**, 1787–1794.
11. Li, J., Bai, Y., Ianakova, E., Grandis, M., Uchwat, F., Trostinskaia, A., Krajewski, K.M., Garbern, J., Kupsky, W.J. and Shy, M.E. (2006) Major myelin protein gene (P0) mutation causes a novel form of axonal degeneration. *J. Comp. Neurol.*, **10**, 252–265.
12. Shames, I., Fraser, A., Colby, J., Orfali, W. and Snipes, G.J. (2003) Phenotypic differences between peripheral myelin protein-22 (PMP22) and myelin protein zero (P0) mutations associated with Charcot-Marie-Tooth-related diseases. *J. Neuropathol. Exp. Neurol.*, **62**, 751–764.
13. Inoue, K., Khajavi, M., Ohyama, T., Hirabayashi, S., Wilson, J., Reggin, J.D., Mancias, P., Butler, I.J., Wilkinson, M.F., Wegner, M. *et al.* (2004) Molecular mechanism for distinct neurological phenotypes conveyed by allelic truncating mutations. *Nat. Genet.*, **36**, 361–369.
14. Parodi, A.J. (2000) Protein glucosylation and its role in protein folding. *Annu. Rev. Biochem.*, **69**, 69–93.
15. Gallagher, M.J., Shen, W., Song, L. and Macdonald, R.L. (2005) Endoplasmic reticulum retention and associated degradation of a GABAA receptor epilepsy mutation that inserts an aspartate in the M3 transmembrane segment of the alpha1 subunit. *J. Biol. Chem.*, **280**, 37995–38004.
16. Niemann, S., Sereda, M.W., Suter, U., Griffiths, I.R. and Nave, K.A. (2000) Uncoupling of myelin assembly and schwann cell differentiation by transgenic overexpression of peripheral myelin protein 22. *Neuroscience*, **20**, 4120–4128.
17. Zhang, K. and Kaufman, R.J. (2006) The unfolded protein response: a stress signaling pathway critical for health and disease. *Neurology*, **66**, S102–S109.
18. Rutkowski, D.T. and Kaufman, R.J. (2004) A trip to the ER: coping with stress. *Trends Cell. Biol.*, **14**, 20–28.
19. Calfon, M., Zeng, H., Urano, F., Till, J.H., Hubbard, S.R., Harding, H.P., Clark, S.G. and Ron, D. (2002) IRE1 couples endoplasmic reticulum load to secretory capacity by processing the XBP-1 mRNA. *Nature*, **415**, 92–96.
20. Doyle, J.P., Stempak, J.G., Cowin, P., Colman, D.R. and D'Urso, D. (1995) Protein zero, a nervous system adhesion molecule, triggers epithelial reversion in host carcinoma cells. *J. Cell Biol.*, **131**, 465–482.
21. Toews, A.D., Fischer, H.R., Goodrum, J.F., Windes, S. and Morell, P. (1987) Metabolism of phosphate and sulfate groups modifying the P0 protein of peripheral nervous system myelin. *J. Neurochem.*, **48**, 883–887.
22. Quarles, R.H. (1997) Glycoproteins of myelin sheaths. *J. Mol. Neurosci*, **8**, 1–12.
23. Filbin, M.T. and Tennekoon, G.I. (1993) Homophilic adhesion of the myelin P0 protein requires glycosylation of both molecules in the homophilic pair. *J. Cell Biol.*, **122**, 451–459.
24. Filbin, M.T. and Tennekoon, G.I. (1991) The role of complex carbohydrates in adhesion of the myelin protein, P0. *Neuron*, **7**, 845–855.
25. De Jonghe, P., Timmerman, V., Ceuterick, C., Nelis, E., De Vriendt, E., Lofgren, A., Vercruyssen, A., Verellen, C., Van Maldergem, L., Martin, J.J. *et al.* (1999) The Thr124Met mutation in the peripheral myelin protein zero (MPZ) gene is associated with a clinically distinct Charcot–Marie–Tooth phenotype. *Brain*, **122**, 81–90.
26. Blanquet-Grossard, F., Pham-Dinh, D., Dautigny, A., Latour, P., Bonnebouche, C., Diraison, P., Chapon, F., Chazot, G. and Vandenberghe, A. (1996) Charcot-Marie-Tooth type 1B neuropathy: a mutation at the single glycosylation site in the major peripheral myelin glycoprotein Po. *Hum. Mutat.*, **8**, 185–186.
27. Sommer, L. and Suter, U. (1998) The glycoprotein P0 in peripheral gliogenesis. *Cell. Tissue Res.*, **292**, 11–16.
28. Martini, R., Zielasek, J., Toyka, K.V., Giese, K.P. and Schachner, M. (1995) Protein zero (P0)-deficient mice show myelin degeneration in peripheral nerves characteristic of inherited human neuropathies. *Nat. Genet.*, **11**, 281–286.
29. Shy, M.E., Arroyo, E., Sladky, J., Menichella, D., Jiang, H., Xu, W., Kamholz, J. and Scherer, S.S. (1997) Heterozygous P0 knockout mice develop a peripheral neuropathy that resembles chronic inflammatory demyelinating polyneuropathy (CIDP). *J. Neuropathol. Exp. Neurol.*, **56**, 811–821.
30. Giese, K.P., Martini, R., Lemke, G., Soriano, P. and Schachner, M. (1992) Mouse P0 gene disruption leads to hypomyelination, abnormal expression of recognition molecules, and degeneration of myelin and axons. *Cell*, **71**, 565–576.
31. Wrabetz, L., D'Antonio, M., Pennuto, M., Dati, G., Tinelli, E., Fratta, P., Previtali, S., Imperiale, D., Zielasek, J., Toyka, K. *et al.* (2006) Different intracellular pathomechanisms produce diverse Myelin Protein Zero neuropathies in transgenic mice. *J. Neurosci.*, **26**, 2358–2368.
32. Dickson, K.M., Bergeron, J.J., Shames, I., Colby, J., Nguyen, D.T., Chevet, E., Thomas, D.Y. and Snipes, G.J. (2002) Association of calnexin with mutant peripheral myelin protein-22 ex vivo: a basis for 'gain-of-function' ER diseases. *Proc. Natl Acad. Sci. USA*, **99**, 9852–9857.
33. Fortun, J., Li, J., Go, J., Fenstermaker, A., Fletcher, B.S. and Notterpek, L. (2005) Impaired proteasome activity and accumulation of ubiquitinated substrates in a hereditary neuropathy model. *J. Neurochem.*, **92**, 1531–1541.
34. Avila, R.L., Inouye, K., D'Antonio, M.L., Feltri, M.L., Wrabetz, L. and Kirschner, D.A. (2007) Roles of Adhesion interfaces and novel disulfide in myelin instability and packing defects in MPZS63C transgenic mice. *J. Peripher. Nerv. Syst.*, **12S**, 6.
35. Manent, J., Oguievetskaia, K., Bayer, J., Ratner, N. and Giovannini, M. (2003) Magnetic cell sorting for enriching Schwann cells from adult mouse peripheral nerves. *J. Neurosci. Methods*, **123**, 167–173.
36. Zacharias, D.A., Violin, J.D., Newton, A.C. and Tsien, R.Y. (2002) Partitioning of lipid-modified monomeric GFPs into membrane microdomains of live cells. *Science*, **296**, 913–916.
37. Qian, Y., Galli, A., Ramamoorthy, S., Risso, S., DeFelice, L.J. and Blakely, R.D. (1997) Protein kinase C activation regulates human serotonin transporters in HEK–293 cells via altered cell surface expression. *J. Neurosci.*, **17**, 45–57.